



# Analysis of superconducting linear synchronous motor for electromagnetic propulsion

Guanchun Li<sup>1</sup> · Xin Wang<sup>1</sup> · Peng Cui<sup>1</sup> · Jie Li<sup>1</sup>

Received: 11 September 2017 / Revised: 3 November 2017 / Accepted: 21 November 2017 / Published online: 29 January 2018  
© Springer Science+Business Media, LLC, part of Springer Nature 2018

## Abstract

There is a high demand for electromagnetic launchers in applications such as electromagnetic catapults and launch-assist systems for spacecraft, owing to their advantages in terms of controllability and reusability. This work proposes a double-sided superconducting-magnet linear synchronous motor capable of large thrust densities that can satisfy the demands of high-load launcher systems. Ring windings and narrow-toothed structures were applied to increase the density of the armature winding and reduce cogging-torque-induced fluctuations, and superconducting magnet with iron-core was first proposed to produce a strong air gap magnetic field. Numerical simulations are used to construct a simulation model of the motor, which is then used to study the relationships between the thrust characteristics of the motor and the dimensions of its armature and air-gap length. The results of this analysis provide information on the optimal thrust characteristics of linear motors in electromagnetic launcher systems.

**Keywords** Electromagnetic launch · Thrust density · Superconducting linear motor · Magnetic saturation

## 1 Introduction

An electromagnetic launcher is a type of electromechanical converter, which uses electromagnetic force to propel loads up to a certain launching speed, according to the principles of interaction between magnetic fields and electric currents. Electromagnetic launchers are in high demand for applications such as launching aircraft from aircraft carriers, railguns, launch-assist systems for spacecraft, and ultrahigh-speed sled tests, as they demonstrate several advantages over conventional steam and chemical launchers, such as high launcher efficiency, excellent controllability, structural diversity, and reusability [1–5]. Currently, the catapult systems used in aircraft carriers are capable of relatively low launch velocities only, which are generally lower than 103 m/s for launch loads weighing less than 22.5 t [6]. The launch velocities of railguns are very high and may reach 9600 m/s, but the masses of the railgun projectiles do not exceed 100 kg [7]. The systems used in electromagnetic traction for rail transit are capable of handling very large loads (approximately 30

t), and speeds up to 603 km/h can be attained using these systems; however, the acceleration in rail transit systems is usually quite low, at  $\sim 1 \text{ m/s}^2$  [8–14]. Increasing levels of attention are thus being paid toward research on linear motors capable of high thrust densities, especially those that address the demands of high mass–ultrahigh-speed applications [15]. To ensure reliability of the launcher during ultrahigh-speed operations, the mechanical air gaps between the mover and the armature in linear motors are generally larger than that in rotary motors [16,17]. However, excessively large air gaps in the motor will reduce the energy efficiency of the linear motor (such that it becomes lower than that of a rotary motor), and weaken the magnetic field in the air gap, which results in low thrust densities. The faster speed of the linear motor, the higher frequency of the armature. High armature frequency not only burden on the power supply system, but also result in large reactive power [18]. So the high thrust density and ultra-high speed linear motor needs to have a strong air gap magnetic field and large pole pitch. Some scholars have proposed variable pole pitch double-sided linear induction motor with ladder-slot-secondary to reduce the armature frequency and improve efficiency [19]. However, the asynchronous characteristics and the skin effect limit the improvement in efficiency and thrust density of induction motor. In order to improve the thrust density of linear

✉ Guanchun Li  
duanpaidou586@yeah.net

<sup>1</sup> Engineering Research Center of Maglev Technology, National University of Defense Technology, Changsha 410073, China

motor, researchers proposed air-core superconducting linear synchronous motor [20]. However, magnetic field of air-core motor diverge in the air. It will lead to magnetic shielding problems and magnetic field utilization is very low. In addition, when the ratio of magnet length and air gap length is large, the magnetic field distribution in the air gap is not uniform, and it makes thrust fluctuate. To overcome this issue, we propose a double-sided iron-core superconducting linear synchronous motor. Iron core is used to connect the magnetic circuits to avoid magnetic field divergence and make the air gap magnetic field uniform. Furthermore, the double-sided structure circumvents the issues caused by the normal forces of the single-sided motors. Over the past few years, the fabrication processes and overall performances of superconducting materials have been improving continuously, and significant progress has been made in the applied technical research on magnets based on high-temperature superconducting tapes. SCMs have been successfully applied in electromagnetic levitation and high-power motors. At the Holloman air force base in the United States, superconducting tapes were used to construct powerful magnetic coils, whose maximum magnetic induction was 6.7 T at the center of the magnet and 2.9 T at a distance of 3 cm from the surface of the magnet. This type of SCM was used as the magnetic source of the maglev system used to modify the facility's rocket sled track. Six tests were performed on the modified system using rocket-propelled sleds, and a maximum operational speed of 186.9 m/s was achieved in these tests [21]. Similar SCMs were used as exciter magnets in the synchronous motors used in Japan's high-speed maglev system, and the 33 t maglev trains driven by these motors were able to achieve a maximum operational speed of 603 km/h.

Generally, linear motors are categorized into two types according to their structural characteristics—short stator (moving coil) motors and long stator (moving magnet) motors. The structure of a moving-coil motor is shown in Fig. 1a. As the armature of the motor acts as the mover in this configuration, power cables must be towed during the movement of the motor to supply electricity to the armature, which causes issues in terms of reliability and safety in such systems; this configuration is thus unsuitable for ultrahigh-speed operations. Furthermore, the costs for installing SCMs along the track are too high, making it unfit for applications in engineering. The structure of a moving-magnet motor is shown in Fig. 1b. This type of motor uses SCMs as its mover, and has its armature and power facilities installed on the ground, which greatly reduces the mass of the mover. The SCM is formed by a cooling chamber and superconducting coil. Prior to launching, the superconducting coil is poised in a superconducting state using coolants, after which the superconductor's switch is turned off and the current leads are removed. As superconducting coils have zero electrical resistance, current will flow continuously within the closed superconducting coil;

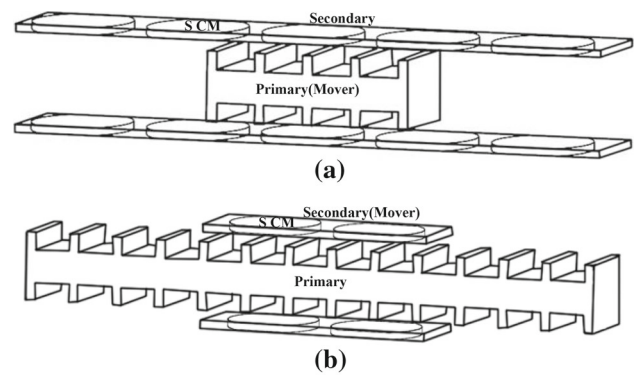


**Fig. 1** Basic structure of a double-sided superconducting-magnet linear synchronous motor (SCLSM). **a** Moving-coil type. **b** Moving-magnet type

therefore, the superconducting coil will not require a continuous supply of electricity during launch, which helps avoid the issues associated with the towing of power cables. In this work, a double-sided SCM linear synchronous motor of narrow-toothed configuration is proposed, to obtain large thrust densities. The effects of magnetic-field distribution and parameters of the aforementioned motor on its thrust characteristics are analyzed using methods based on 3D finite element analysis. The set of parameters that can provide optimal thrust performance can be obtained from the analysis results.

## 2 Analysis of thrust characteristics

### 2.1 Magnetic circuit of motor

The magnetic circuits of the double-sided superconducting linear motor can be classified into two types, according to the magnetic fluxes of the double-sided SCMs: a serial magnetic circuit as shown in Fig. 2a and a parallel magnetic circuit as shown in Fig. 2b. Under normal conditions, the serial magnetic circuit will generate larger thrusts with smaller fluctuations [22,23]. Therefore, the double-sided superconducting linear synchronous motor discussed in this work is analyzed based on serial magnetic circuits.

### 2.2 Thrust analysis

The upper limit of thrust that can be generated in conventional iron-core electric motors is the electromagnetic force that the iron-core material (especially in the teeth) generates at saturation. Any further increase in armature current will not result in an accompanying increase in the electromagnetic force generated by the iron core of the motor. For the double-sided SCLSM, the ring windings have been used for modularizing. The thrust of the motor is the ampere force

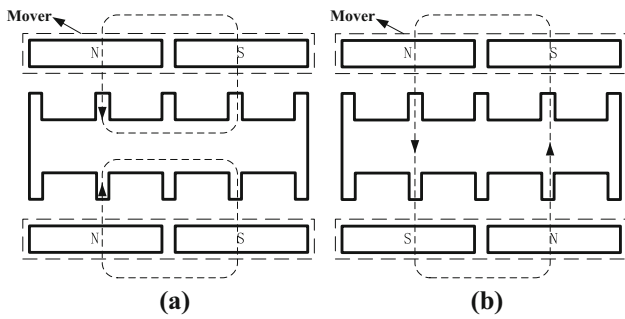


**Fig. 2** Two types of magnetic circuits. **a** Serial magnetic circuit. **b** Parallel magnetic circuit

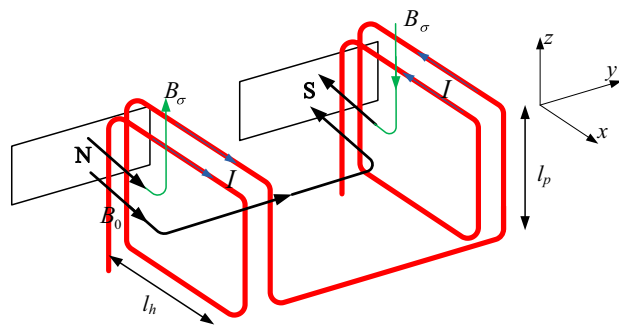


**Fig. 3** Schematic model of the SCLSM

generated by the interactions between the exciting magnetic field and the conducting wires of the armature, and the iron cores simply act as conduits for connecting the magnetic circuits. Therefore, the motor can work in a state where the iron core is highly saturated. Furthermore, the use of narrow-toothed structures can increase the density of the armature winding and reduce cogging-torque-induced fluctuations.

A schematic model of the operating principle of the motor is shown in Fig. 3. Large portions of the magnetic lines of force in the motor are bound to its iron core, and form a closed magnetic circuit by passing through the N and S magnetic poles. When electric current passes through the armature, thrust is generated by the interactions between the magnetic flux density of the air-gap,  $B_0$ , and the perpendicular side  $l_p$  (z-axis in Fig. 3) of the armature’s coils. Simultaneously, a small quantity of magnetic flux leaks from the top and bottom of the iron core and forms a closed magnetic circuit. The leakage magnetic flux density  $B_\sigma$  interacts with the horizontal side  $l_h$  (x-axis in Fig. 3) of the armature’s coils to produce electromagnetic resistance. According to the definition of magnetic force, the average thrust generated by the motor is:

$$F_{av} = pNB_{0av}Il_p - pNB_{\sigma av}Il_h = pNI(B_{0av}l_p - B_{\sigma av}l_h) \tag{1}$$

In (1),  $p$  is the number of magnetic poles,  $N$  is the number of armature turns,  $B_{0av}$  is the average air-gap magnetic flux density,  $B_{\sigma av}$  is the average leakage magnetic flux density,  $I$  is the armature current,  $l_p$  is the height of the armature coil (length of the perpendicular side), and  $l_h$  is the width of the armature coil (length of the horizontal side).

Thrust density is an important indicator for weighing parameters of a motor. When the thrust density reaches its maximum, it is implied that the charge parameters have been optimized. The thrust density of a linear motor is defined as:

$$\rho_F = \frac{F_{av}}{V} = \frac{F_{av}}{l_p l_x (l_h + 2g + 2w)} \tag{2}$$

In (2),  $V$  is the volume of the magnetically coupled parts in the primary coil,  $g$  is the airgap of the motor,  $w$  is the thickness of the SCM, and  $l_x$  is the length of the magnetically coupled parts in the primary coil.

### 3 Finite element model

The finite element model of the SCM linear synchronous motor (SCLSM) is shown in Fig. 4. The simulation model includes four superconducting magnetic poles and a two-phase armature winding; the parameters of the motor are shown in Table 1. ANSYS Maxwell, an electromagnetic-field simulation software, is used for the simulation. Lines A and B along the armature winding’s surface in the finite element model are used to observe the leakage flux density  $B_\sigma$  and the flux density in the airgap,  $B_0$ , in the motor.

### 4 Analysis of finite element simulation

Because of the magnetization characteristics of iron-based magnetic materials, excessively high excitation magnetic fields can saturate iron cores of a motor. Iron-core saturation is a phenomenon that must be avoided at all costs in conventional motor design, as it makes the energy conversion efficiency of the motor low, and leads to overheating of the motor, causing thermal aging of the insulation. However, the thrust of the proposed motor is the ampere force, and the iron cores simply act as conduits for connecting the magnetic circuits to avoid magnetic field divergence. Energy conversion efficiency does not decrease with the saturation of the motor. The motor can work in a state where the iron core is highly saturated. The permeability of ferromagnetic material decreases as the degree of saturation increases, and it will cause the leakage flux densities increase. Therefore, large thrust densities can be obtained by appropriately designing the parameters of motor such that improve the air gap flux density, reduce leakage flux density.

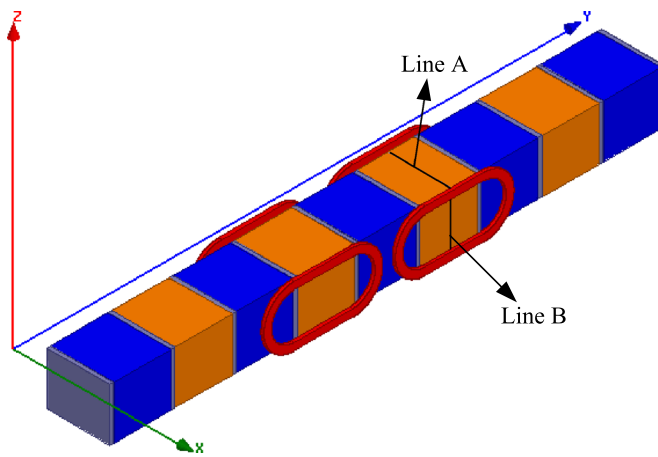


Fig. 4 Model of the moving-magnet SCLSM

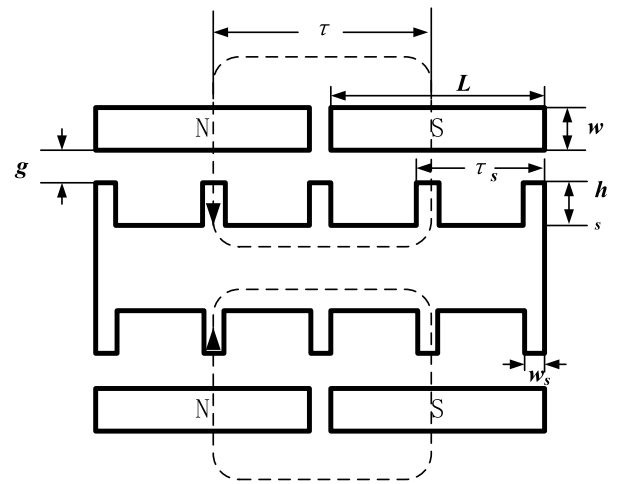


Table 1 Machine design parameters for the SCLSM

Symbol	Item	Value
$\tau$	Pole pitch	1.04 m
$g$	Length of air gap	0.01 mm
$\tau_s$	Slot pitch	0.485 m
$w_s$	Width of slot	0.03 m
$h_s$	Depth of slot	0.02 m
$I$	Rare current	2000 A
$N$	Turns of armature	10
$I_{sc}$	Current of SCM	210 A
$N_{sc}$	Turns of SCM	2340
$L$	Length of SCM	0.94 m
$h$	Height of SCM	0.48 m
$w$	Thickness of SCM	0.0254 m
	Material of core	Steel

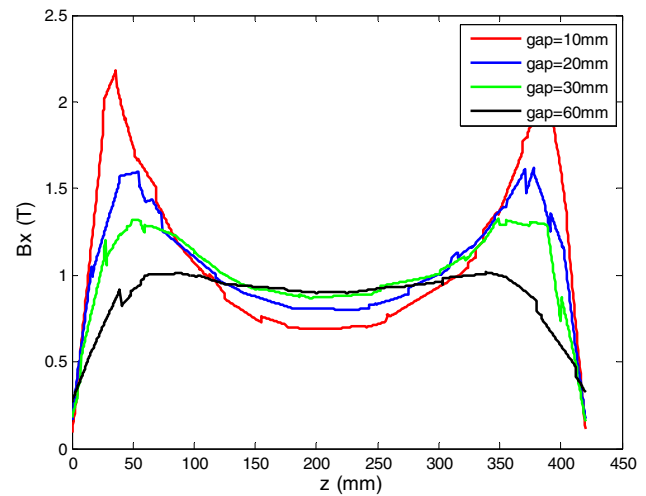


Fig. 5 Magnetic field distributions of air-core superconducting magnet

### 4.1 Magnetic field distributions of superconducting magnet

The parameters of superconducting magnet is shown in Table 1. Figure 5 shows the magnetic field distributions of a air-core superconducting magnet. In Fig. 5, it is shown that the magnetic field distribution of the air-core superconducting magnet is not uniform. The magnetic density on the two sides is much higher than that of center parts. Because when the length of the magnet pole is much larger than the air gap length, the magnetic density of center part is depressed. And the smaller the air gap, the more obvious this phenomenon. Figure 6 shows the comparison of the magnetic field distribution between the iron-core and air-core superconducting magnet with different air gap length. It can be seen from the Fig. 6, the magnetic field distribution of iron-core superconducting magnet is more uniform and stronger, and the

magnetic density is two times air-core superconducting magnet. And the air gap magnetic field decreases very little as the air gap length increases, so the motor can work under a large gap length.

### 4.2 Magnetic flux density distribution in the motor

The air-gap length and the height and width of the armature are defined as  $g = 0.035$  m,  $l_p = 0.42$  m, and  $l_h = 0.5$  m, respectively. The magnetic flux density distributions of the motor are illustrated in Fig. 7a and b showing the magnetic flux density distributions of the main magnetic circuit and magnetic leakage circuit of the motor, respectively. In Fig. 7a, it is shown that the main magnetic circuit of the motor is closed by passing through two SCMs on the same side; the magnitude of the iron core’s magnetic density is approximately 2 T. The point of maximum magnetic flux density of

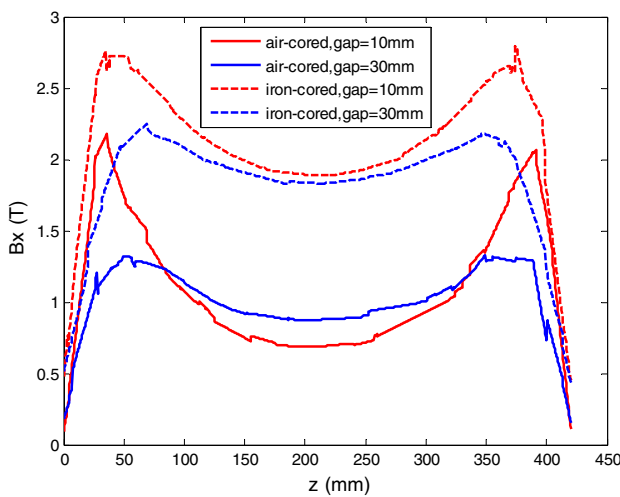


**Fig. 6** Comparison of the magnetic field distribution between the iron-core and air-core superconducting magnet

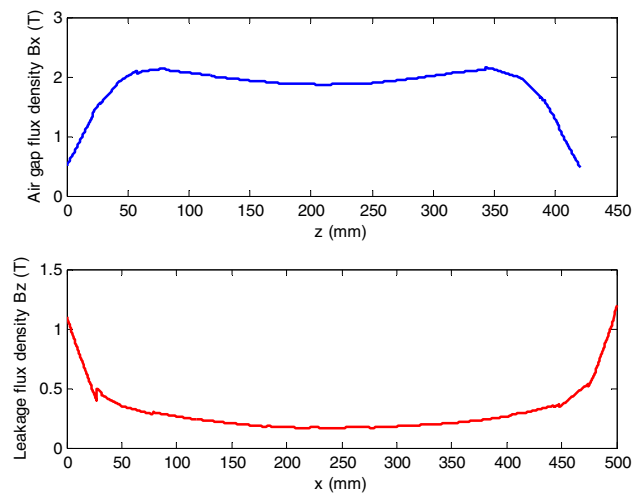


**Fig. 8** Air-gap flux density and leakage flux density

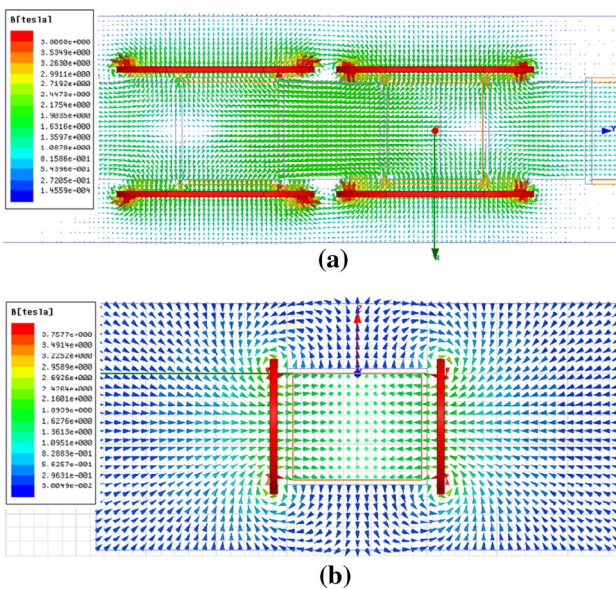


**Fig. 7** Magnetic field distributions of the SCLSM

the air gap is located on the surface of the SCMs’ terminals, at approximately 3.8 T. The magnitude of the leakage flux density of the flux that flows out of the iron core’s top and bottom faces is approximately 0.2 T. The effective magnetic flux density in the air gap (the magnetic flux density distribution in the  $x$ -direction above Line B) and the leakage flux density (the magnetic flux density distribution in the  $z$ -direction above Line A) are shown in Fig. 8. In particular, the average value of magnetic flux density in the air gap is 1.84 T whereas the average leakage flux density is 0.30 T. The leakage flux increases in severity with decreasing distance from the SCM. The leakage flux density is 16.3% of the air-gap’s magnetic flux density. The electromagnetic thrust generated by these four SCMs is 64.8 kN, with a thrust density of 109.83 kN/m<sup>3</sup>.

Although the leakage flux density is big, but the linear motor still has a great thrust density because of the ring winding.

### 4.3 Effects of air-gap length

Figures 6, 7, and 8 present the results of time and temperature at maximum pore pressure in different depths. From Fig. 6, it can be observed that the maximum pore pressure occurs during 13–19 min in the depth of 10 mm during exposed to ISO 834 fire curve, while the range of temperature at maximum pore pressure is about 200–280 °C. The addition of fibers prolongs the time of observing the maximum pore pressure in all depths. For all series, the pore pressure at the depth of 30 mm is the highest. As shown in Fig. 8, it is further importantly observed that the maximum pore pressure occurred in the temperature ranges of 200–230 °C. It seems that the pore pressure relief occurs after melting of PP fibers, since the melting temperature of PP fiber is around 170 °C. This observation is somehow different with M.R. Bangi’s results. The difference of heating pattern (electric radiant heater and fire) and heating rate may lead to this distinction.

The armature’s height is defined as  $l_p = 0.42$  m and its width is defined as  $l_h = 0.5$  m. The relationship between the electromagnetic thrust and the length of the air gap is shown in Fig. 9. The electromagnetic thrust reaches its peak at 65.12 kN when the air-gap length is 30 mm. The changes in the air-gap flux density and leakage flux density with changes in the length of the air gap are shown in Figs. 10 and 11, respectively. It is observed that the magnetic field in the air gap increases in strength as the air-gap length decreases; however, a large decrease in the air-gap length increases the leakage flux density. Therefore, the relationship between the electromagnetic force and the length of the air gap is not linear. There is an optimal air gap that maximizes the output thrust of the motor.

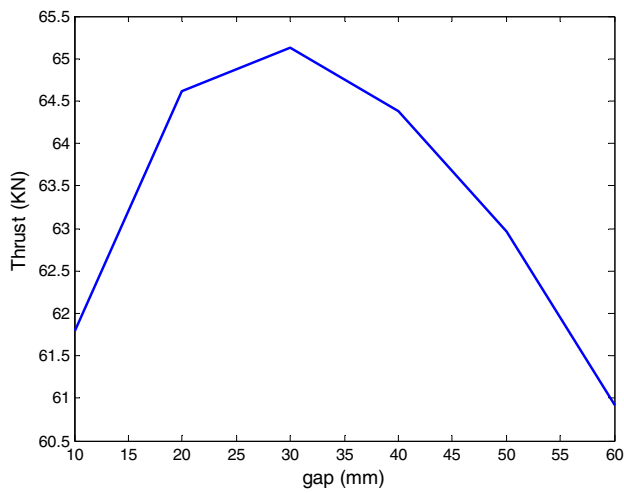


Fig. 9 Thrust curves for different air-gap lengths

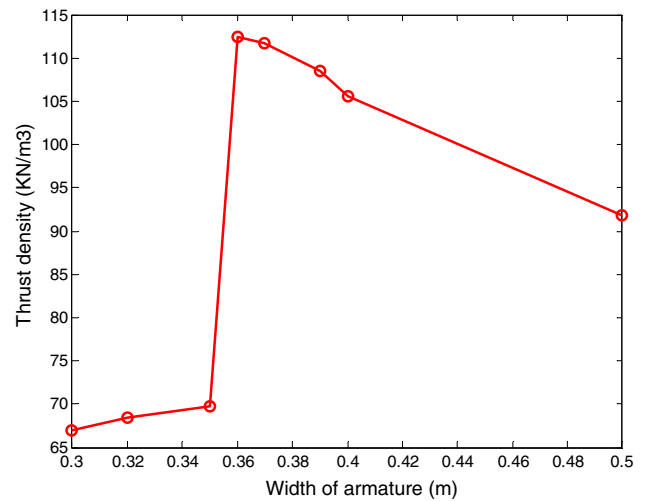


Fig. 12 Relationship between thrust density and armature width

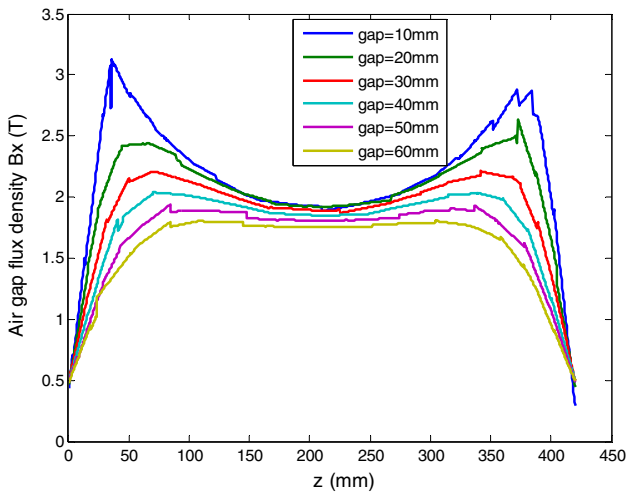


Fig. 10 Air-gap flux density for different air-gap lengths

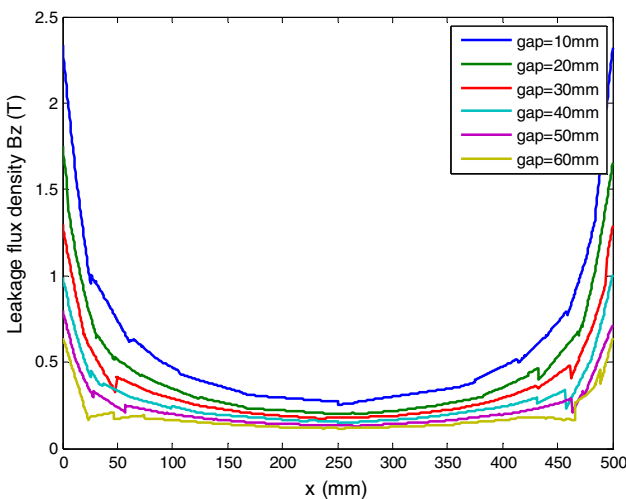


Fig. 11 Leakage flux density

### 4.4 Effects of armature width

In (1), it can be observed that the horizontal sides of the armature coil do not produce electromagnetic thrust; instead, they generate resistance because of the effects of the leakage flux density. Therefore, excessively wide armature coils may lead to high resistance and cause the volume of the armature to become very large. The air-gap length is defined as  $g = 0.030$  m, while the armature's height is defined as  $l_p = 0.42$  m. The relational plot between armature width and thrust density is shown in Fig. 12, while the relationships between the width of the armature and the average air-gap and leakage flux densities are shown in Fig. 13. Figure 12 shows that the thrust density is the maximum when the width of the armature is 360 mm. At armature widths narrower than 360 mm, the iron cores become saturated, which results in significant increases in the leakage flux and a rapid decrease in the thrust density.

### 4.5 Effects of armature height

The armature height is the length of the perpendicular side of the motor. The length of the air gap, width of the armature, and height of the SCMs are defined as  $g = 0.030$  m,  $l_h = 0.4$  m, and  $h = 0.48$  m, respectively. Figure 14 shows the relationship plot between the height of the armature and thrust density, while the relationships of the height of the armature with the average air gap and leakage flux densities are illustrated in Fig. 15. The results of the simulation demonstrate that the thrust density initially increases and then decreases as the armature height increases. A maximum thrust density of  $107.4 \text{ kN/m}^3$  is attained for an armature height of 380 mm. The thrust density decreases when the height of the armature exceeds that of the SCMs. The distribution of the magnetic flux density in the air gap along the

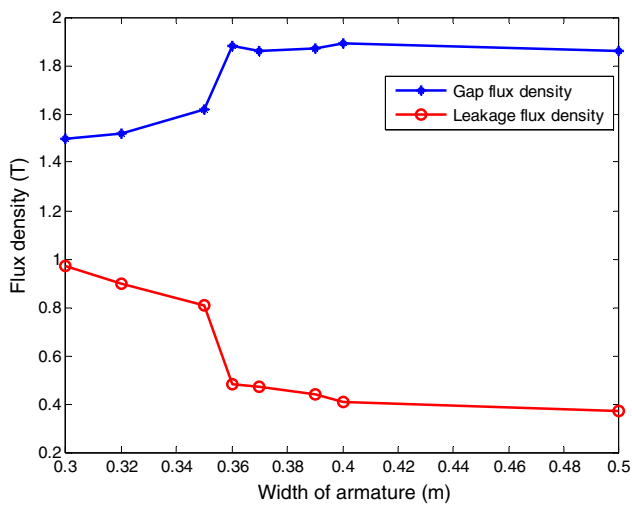


**Fig. 13** Relationships of average gap flux density and leakage flux density with armature width

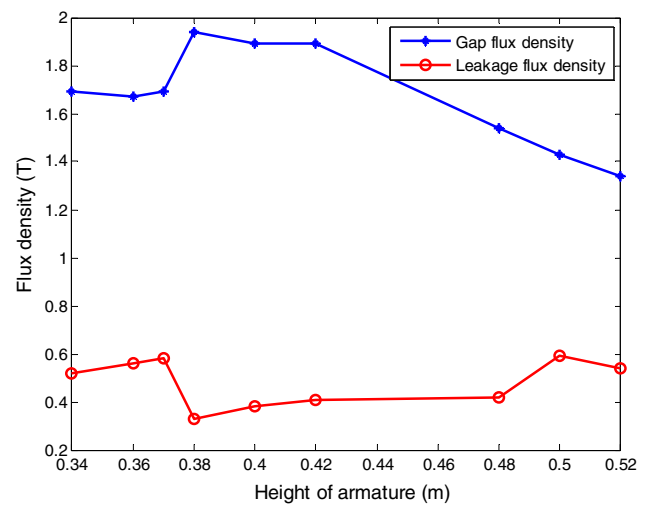


**Fig. 15** Average gap flux density and leakage flux density versus armature height

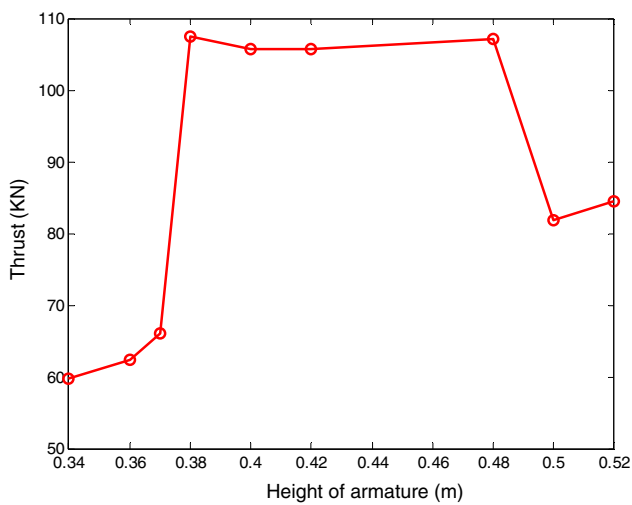


**Fig. 14** Thrust versus armature height

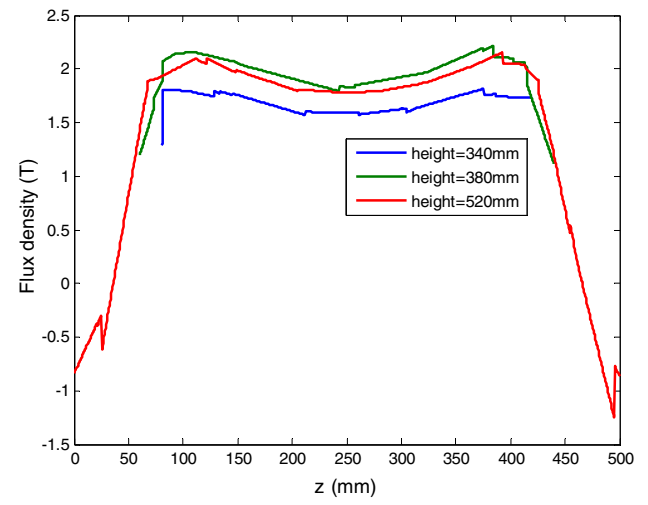


**Fig. 16** Distribution of magnetic flux density

perpendicular sides (Line B) of the armature coil is shown in Fig. 16. In this figure, it is shown that the magnetic field changes from positive to negative at the upper and lower ends of the armature’s perpendicular sides, which causes the electromagnetic force to change from thrust into resistance.

### 5 Conclusion

Electromagnetic launch systems feature high power densities over short periods. Linear motors, which are the actuators of these systems, must thus possess very large thrust densities. A type of superconducting linear motor was proposed in this work, which ring windings and iron core have been used to enabled the linear motor to fully utilize the powerful magnetic fields generated by the SCMs and produce large

thrust densities. A finite element simulation model of the motor was also constructed in this work, which was used to describe the magnetic field distributions of the motor, and to study the relationships of the thrust characteristics with the length of the air gap and armature dimensions. The set of parameters that results in optimal motor performance can be analyzed from the results of these simulations. Superconducting linear motors with narrow-teeth configurations overcome the limitations of thrust observed in conventional iron-core motors and the magnetic-field dispersion in air-core motors. The eddy current effect in the iron core is still a problem at ultrahigh speeds, and the suppression of this eddy current effect will be the subject of further research.

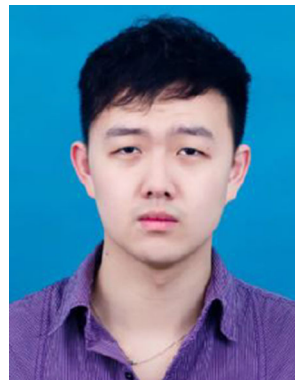
**Acknowledgements** This work was supported by the Weapons Prediction Fund Project of the General Equipment Department (Grant No. 9140A20101015KG01).

## References

- Ma, W.M., Lu, J.Y.: Electromagnetic launch technology. *J. Natl. Univ. Def. Technol.* **38**(6), 1–5 (2016)
- Zhang, Z., Zhou, H., Duan, J., et al.: Research on permanent magnet linear synchronous motors with ring windings for electromagnetic launch system. *IEEE Trans. Plasma Sci.* **45**(7), 1161–1167 (2017)
- Bertola, L., Cox, T., Wheeler, P., et al.: Electromagnetic launch systems for civil aircraft assisted take-off. *Arch. Electr. Eng.* **64**(4), 535–546 (2015)
- Valentini, G.L.: An overview of energy efficiency techniques in cluster computing systems. *Cluster Comput.* **16**(1), 3–15 (2013)
- Mingyuan, Z., Weiming, M., Guangsen, W.: Overview on a significant technology of modern aircraft carrier-electromagnetic aircraft launch system. *Ship Sci. Technol.* **35**(10), 1–5 (2013)
- Gorazd, S., Mehmet, T.A., Damir, Z., Thomas, A.L.: Design of a linear bulk superconductor magnet synchronous motor for electromagnetic aircraft launch. *IEEE Trans. Appl. Supercond.* **14**(1), 54–62 (2004)
- Skurdal, B.D., Gaigler, R.L.: Multimission electromagnetic launcher. *IEEE Trans. Magn.* **45**(7), 2622–2627 (2010)
- Zhao, J., Hu, H., Liu, X., et al.: Influence of edge permanent-magnet shape on the performance of an arc-linear permanent-magnet synchronous machine. *IEEE Trans. Magn.* **51**(11), 1–4 (2015)
- Park, C.B., Lee, B.S., Lee, C.Y.: Characteristic analysis of superconducting LSM for the wheel-rail-guided very high speed train according to winding method of the ground 3-phase coils. *Trans. Korean Inst. Electr. Eng.* **63**(8), 1164–1169 (2014)
- Perl, A., Goetz, A.: Getting up to speed: assessing usable knowledge from global high-speed rail experience for the United States. *Transp. Res. Rec.* **2475**, 1–7 (2015)
- Sato, K.: High-speed positioning of ultrahigh-acceleration and high-velocity linear synchronous motor. *Int. J. Precis. Eng. Manuf.* **15**(8), 1537–1577 (2014)
- Wu, Z.H., Jin, J.X.: Characteristic analysis of HTS linear synchronous generators designed with HTS bulks and tapes. *IEEE Trans. Appl. Supercond.* **24**(5), 1–5 (2014)
- Carretero, J., Blas, J.G.: Introduction to cloud computing: platforms and solutions. *Cluster Comput.* **17**(4), 1225–1229 (2014)
- Wang, Y., Luo, W., Yan, Z.: Review on multipole field electromagnetic launching technology. *High Volt. Eng.* **40**(4), 1165–1172 (2014)
- Ma, W.M., Wang, D., Chen, S.W., Chen, J.Q.: Common basic scientific problems and development of leading-edge technology of high performance motor system. *Proc. CSEE* **36**(8), 2025–2035 (2016)
- Lu, J.Y., Ma, W.M., Xu, J.: Modeling and simulation of high speed long primary double-sided linear induction motor. *Proc. CSEE* **28**(27), 89–94 (2008)
- Abdollahi, S.E., Mirzayee, M., Mirsalim, M.: Design and analysis of a double-sided linear induction motor for transportation. *IEEE Trans. Magn.* **51**(7), 1–7 (2015)
- Ma, W.M., Xiao, F., Nie, S.X.: Applications and development of power electronics in electromagnetic launch system. *Trans. Chin. Electrotech. Soc.* **31**(19), 1–10 (2016)
- Di, J., Fan, Y., Liu, Y.J., Liu, S.J., Zhu, Y.L.: Variable pole pitch electromagnetic propulsion with ladder-slot-secondary double-sided linear induction motors. *Appl. Sci.* **7**, 481–493 (2017)
- Park, C.B., Lee, B.S., Lee, C.Y.: Characteristic analysis of superconducting LSM for the wheel-rail-guided very high speed train according to winding method of the ground 3-phase coils. *Trans. Korean Inst. Electr. Eng.* **63**(7), 1164–1169 (2014)
- Su, Y.H., Langhorn, A., Ketchen, D., Holland, L., Minto, D., Doll, D.: Magnetic levitation upgrade of the Holloman high speed test track. *IEEE Trans. Appl. Supercond.* **19**(3), 2074–2077 (2009)
- Cheshmehbeigi, H.M., Khanmohamadian, A.: Design and simulation of a moving magnet type linear synchronous motor for electromagnetic launch system. *Int. J. Eng. Trans. C* **30**(3), 351 (2017)
- Li, L.Y., Ma, M.N., Kou, B.Q., Chen, Q.Q.: Analysis and design of moving-magnet-type linear synchronous motor for electromagnetic launch system. *IEEE Trans. Plasma Sci.* **39**(1), 121–126 (2011)



**Guanchun Li** received the B.S. degree in automation from Donghua University, Shanghai, China, in 2011. He is currently working toward his Ph.D. degree in the Engineering Research Center of Maglev Technology. His research interests include hypersonic propulsion technology and linear synchronous motor control technology.



**Xin Wang** received the M.S. degree from Lanzhou University, Lanzhou, China, in 2013. He is currently working toward his Ph.D. degree in the Hunan University. His research interest is Mechanical Engineering.



**Peng Cui** received the Ph.D. degree in automation from National University of Defense Technology, Changsha, China, in 2010. His research interests include maglev control technology and linear synchronous motor control technology.





**Jie Li** received the Ph.D. degree in automation from National University of Defense technology, Changsha, China, in 1999. He carried out his postdoctoral research at Hong Kong University of Science and Technology. Now, he is a professor with the Engineering Research Center of Maglev Technology. His research interests include robotics and maglev control technology.